Journal of Thermal Analysis, Vol. 29 (1984) 491–502

KINETIC STUDY OF THE THERMAL DECOMPOSITION OF COBALT(III) OXYHYDROXIDE
II. Thermogravimetric, textural and structural data

*L. Hernan, J. Morales, A. Ortega** and *J. L. Tirado*

DEPARTAMENTO DE QUÍMICA INORGÁNICA, FACULTAD DE CIENCIAS, UNIVERSIDAD DE CÓRDOBA, SPAIN

(Received January 24, 1984)

The kinetics of thermal decomposition of CoOOH under vacuum have been studied by the analysis of dynamic weight loss data. The comparison of the values of activation energy computed from the application of different methods of TG data analysis and those obtained in isothermal conditions, allows to detect a first order law as the most suitable mechanism for the reaction. Nevertheless, there is no clear differentiation between this model and those based in contracting geometry equations. The discrimination of the formal kinetics governing this reaction has been made on the basis of X-ray profile analysis and electron microscopy results. The reaction seems to occur by a random nucleation process that leads to the formation of cracks, which confine coherently scattering domains of 50–100 Å. The occurrence of these isolated blocks might account for a rate of decomposition proportional to the amount of undecomposed reactant.

In part one of this paper [1], we have discussed how the isothermal gravimetric procedures of kinetic analysis are unable to yield a precise mechanism for the complex reaction of thermal decomposition of CoOOH, that develops according to the process (1),

$$12\ CoOOH \longrightarrow 4\ Co_3O_4 + 6\ H_2O + O_2 \qquad (1)$$

since the data can be fitted satisfactorily to several kinetic rate laws which lead to similar activation energies.

In contrast, different authors [1, 3] have shown that the value of activation energy obtained from the analysis of a thermogravimetric curve considerably depends on the choice of kinetic expression. In this respect, the comparison of kinetic parameters obtained under isothermal and dynamic temperature conditions could provide a significant test in the distinguishability of the mechanism of the reaction.

Here we report on the kinetic information obtained from the thermal decomposition of CoOOH in vacuum from non-isothermal measurements. Microscopic, textural and structural examinations were also performed in order to have a more complete knowledge on the formation of the spinel Co_3O_4.

* Present address: Departamento de Química Inorgánica, Facultad de Química, Universidad de Sevilla, Spain.

Experimental

The experimental method used for the TG runs – a Cahn RG electrobalance attached to a high vacuum system – was identical to that used for the isothermal runs. Powder samples (*ca.* 10 mg), prepared as described in part I, were used to record the TG curves at different constant heating rates.

Electron micrographs were obtained with a Siemens Elmiskop 102 apparatus. Samples were dispersed in acetone by ultrasound and settled on copper grids covered with a holey carbon film.

N_2 adsorption isotherms at 77 K were determined in a Pyrex high vacuum apparatus and the dead spaces with He gas. Pressures were measured by a digital manometer Balzers APR-010 within an accuracy of 0.1 mbar. Specific surface area was calculated by the BET [4] method.

X-ray diffraction patterns were recorded on a Phillips PW 1130 diffractometer, using CoK_α radiation and Fe filter. X-ray diffraction line profiles were recorded by continuous scan at 0.125° min^{-1} and the intensities were read each 0.025°2θ. Line profile analysis was carried out in the (111), (220) and (511) reflections of Co_3O_4. These lines were chosen by their high peak to background ratio excluding overlapping peaks. A highly crystalline Co_3O_4 sample (CoOOH annealed at 850° for 2 hours) provided the instrumental profiles. Centroid position and background level were corrected by means of a computer program based on that of Edwards and Toman [5].

The determination of crystallite size and microstrains was elaborated by the variance method. From the slope (k) and intercept (Wo) of the variance-range curves of the g and h profiles corrected for truncation [6], the slope and intercept of the f profiles were obtained. Slopes were simply subtracted while the intercepts were corrected for the non-additivity error:

$$k_f = k_h - k_g$$
$$Wo_f = Wo_h - Wo_g - \frac{\pi^2 k_f k_g}{2} \qquad (2)$$

The values of k_f and Wo_f were used in the computation of apparent crystallite size (ϵ_k) and the variance of the lattice strain distribution ($\langle e^2 \rangle$), by means of the equation of Langford and Wilson [7], in which:

$$k_f = \frac{\lambda}{\pi^2 \epsilon_k \cos\theta}$$
$$Wo_f = 4 \tan^2\theta \langle e^2 \rangle - \frac{\lambda^2}{4\pi^2 \epsilon_k^2 \cos^2\theta} \qquad (3)$$

where λ is the radiation wavelength and θ the angle of the line centroid.

Results and discussion

TG curves recorded at various heating rates are collected in Fig. 1. These data were processed to give the activation energy of reaction (1) by using the Coats and Redfern approach [8] extended to the nine kinetic rate laws used in the fitting of isogravimetric data. Fig. 2a and b shows the resulting computer plots for the extremes in heating rate. The values of activation energy and linear regression coefficients obtained by the least-squares method are listed in Table 1. As can be observed, high correlation coefficients result from the analysis of TG traces obtained at low heating rates. On increasing the heating rate, the plots of the Coats and Redfern equation [8] show a change in the slope located at *ca.* $\alpha = 0.7$ (Fig. 2b) – especially for the diffusion mechanisms –,

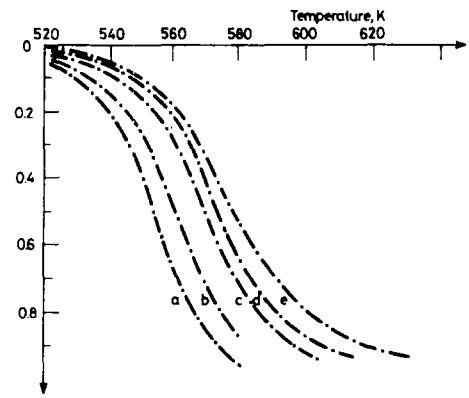

Fig. 1 TG curves of the thermal decomposition of CoOOH at various heating rates, a) 2, b) 4, c) 6, d) 8 and e) 10 deg min^{-1}

which is reflected in the linear correlation coefficients (see Table 1). This Table also reveals that the values of E_a decrease as heating rate increase. A similar behaviour has been found by Gallagher et al. [9] in the study of the kinetics of the thermal decomposition of $CaCO_3$. As suggested by these authors, working at low heating rates, a better thermal equilibrium is reached and dynamic data may approach those of isothermal measurements. Thus, a fair agreement with the conclusions obtained from isothermal results can be expected at low heating rates.

From the results in Table 1, statistical methods such as the F-test and *t* critical ratio were insensitive to decide which kinetic equation gave the most acceptable fit. However, if we compare the values of activation energy in Table 1 with that obtained under isothermal conditions – 193 kJ $mole^{-1}$ –, the rate laws labelled A_2, A_3 – Avrami–Erofeev equations – and D_1, D_2, D_3, D_4 – diffusion mechanisms – can be discarded as operative mechanisms in the formation of the spinel Co_3O_4, since a clear discrepancy appears in these values.

The distinguishability among the kinetic expressions based on the concept of reaction – labelled F_1, R_2 and R_3 in Table 1 – is more difficult, especially for those

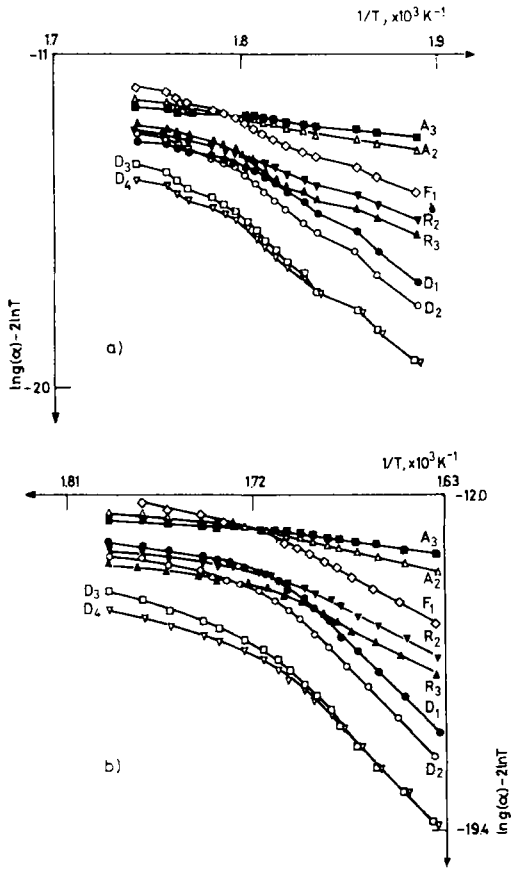

Fig. 2 Plot of ln $(g(\alpha)) - 2$ Ln T *vs.* $1/T$ (method of Coats and Redfern). a) $a = 2$, b) $a = 10$ deg min^{-1}

labelled F_1 and R_2, as a result of the sequence that heating rate imposes to the activation energy values.

Plots like Fig. 2b, obtained from a TG curve recorded at 6 deg min^{-1}, have been used by Avramov [10] to point out that reaction (1) proceeds according to a R_2 contracting area mechanism with two stages of different activation energies. This conclusion was criticized in the first part of this paper. The new results reported here support our doubts on the assumptions of Avramov.

The thermogravimetric curves of Fig. 1 were also analyzed according to the method proposed by Ozawa [11]. The method is based on the effect of the heating rate on thermogravimetric curves and has the advantage over the Coats and Redfern approach [8] that the knowledge of the mechanism, more accurately the $g(\alpha)$ function, is not a prerequisite. Typical plots of this procedure are given in Fig. 3. The activation energies calculated from the slope of these plots are collected in Table 2, together with those obtained by applying the Kissinger method [12] to TG curves.

Table 1 Linear regression coefficients and activation energy values obtained by the application of Coats and Redfern method to the thermogravimetric traces in Fig. 1

Mechanism		$a =$ 2	4	6	8	10
F_1	r	− 0.9959	− 0.9960	− 0.9880	− 0.9820	− 0.9773
	E_a	171	168	151	147	124
A_2	r	− 0.9952	− 0.9951	− 0.9872	− 0.9794	− 0.9730
	E_a	81	79	71	69	57
A_3	r	− 0.9947	− 0.9959	− 0.9852	− 0.9761	− 0.9673
	E_a	51	50	44	44	35
R_2	r	− 0.9911	− 0.9869	− 0.9760	− 0.9652	− 0.9578
	E_a	143	140	125	122	102
R_3	r	− 0.9931	− 0.9910	− 0.9807	− 0.9724	− 0.9652
	E_a	151	149	133	130	109
D_1	r	− 0.9821	− 0.9762	− 0.9618	− 0.9494	− 0.9391
	E_a	249	243	217	212	177
D_2	r	− 0.9884	− 0.9840	− 0.9720	− 0.9609	− 0.9531
	E_a	277	271	243	237	199
D_3	r	− 0.9936	− 0.9911	− 0.9824	− 0.9740	− 0.9681
	E_a	313	307	275	270	227
D_4	r	− 0.9905	− 0.9873	− 0.9763	− 0.9652	− 0.9580
	E_a	289	283	254	247	209

E_a in kJ mol^{-1}, a in deg min^{-1}

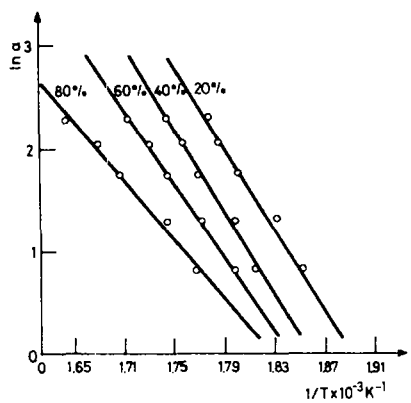

Fig. 3 Plots of logarithms of heating rate *versus* reciprocal absolute temperature at different degrees of decomposition

The comparison of these values with those of Table 1 and with isothermal results corroborates the suppositions made above. In the first instance, the most suitable mechanism for the CoOOH decomposition can be postulated as a random nucleation

Table 2 Activation energies of the decomposition of CoOOH calculated by the Ozawa and Kissinger procedures

Degree of decomposition	E_a, kJ/mol	Degree of decomposition	E_a, kJ/mol
0.1	168	0.6	160
0.2	166	0.7	141
0.3	178	0.8	121
0.4	178	0.9	102
0.5	173	Mean	154

Kissinger method ($\alpha_{max} = 0.5$) 167

of small particles for which the rate of reaction is proportional to the amount of undecomposed CoOOH. Nevertheless, random and systematic errors, which can affect the kinetic measurements, prevent a clear differentiation between this F_1 model and phase-boundary mechanisms in which the rate of decomposition is governed by the progression of an interface spinel-oxyhydroxide towards the centre of the crystal.

At this point, it is noteworthy to examine the evolution of textural and structural characteristics of microcrystals at different stages of the reaction, in order to get a parallel information which could clarify the true mechanism.

Figure 4a shows the electron micrograph of undecomposed microcrystals of CoOOH. Its particles appear as thin hexagonal plates of *ca.* 2500 Å wide. However, it must be noted that there is no complete homogeneity in particle size and shape, probably due to differences in crystal growth inside the pressure vessel used to improve CoOOH crystallinity. N_2 adsorption measurements (see Fig. 5△) yield a value of BET surface of 14.9 m^2g^{-1}. The desorption branch of the isotherm in Fig. 5 does not show hysteresis loop, indicative of an unporous material, a conclusion supported by Fig. 4a.

When the oxyhydroxide is partially transformed into Co_3O_4, the particles show the same habit as the undecomposed microcrystals but a complex texture is developed, as revealed by the electron micrographs (see Fig. 4b and c). N_2 adsorbed volume increases notably at this stage – BET surface is now 60.6 m^2g^{-1} – and hysteresis is detected in the desorption branch of the isotherm (Fig. 5○). This phenomenon could be related to the presence of a pore system that in the light of the electron micrographs appears to be originated by a development of cracks with no prefered orientation. Now the crystals seem to be built up of domains of 50–100 Å defined by the lines associated with cracks. If these domains scatter the X-ray coherently, their apparent size can be computed from line broadening analysis. Unfortunately, X-ray diffraction line profile analysis can not be performed in this sample because of peak overlapping problems of the CoOOH and Co_3O_4 reflections. Nevertheless, when reaction (1) is just completed (300°, see Fig. 4d), the appearance of microcrystals is similar to that found at 230°. Thus, the values of crystallite size obtained at 300° could roughly approach to those produced at 230°.

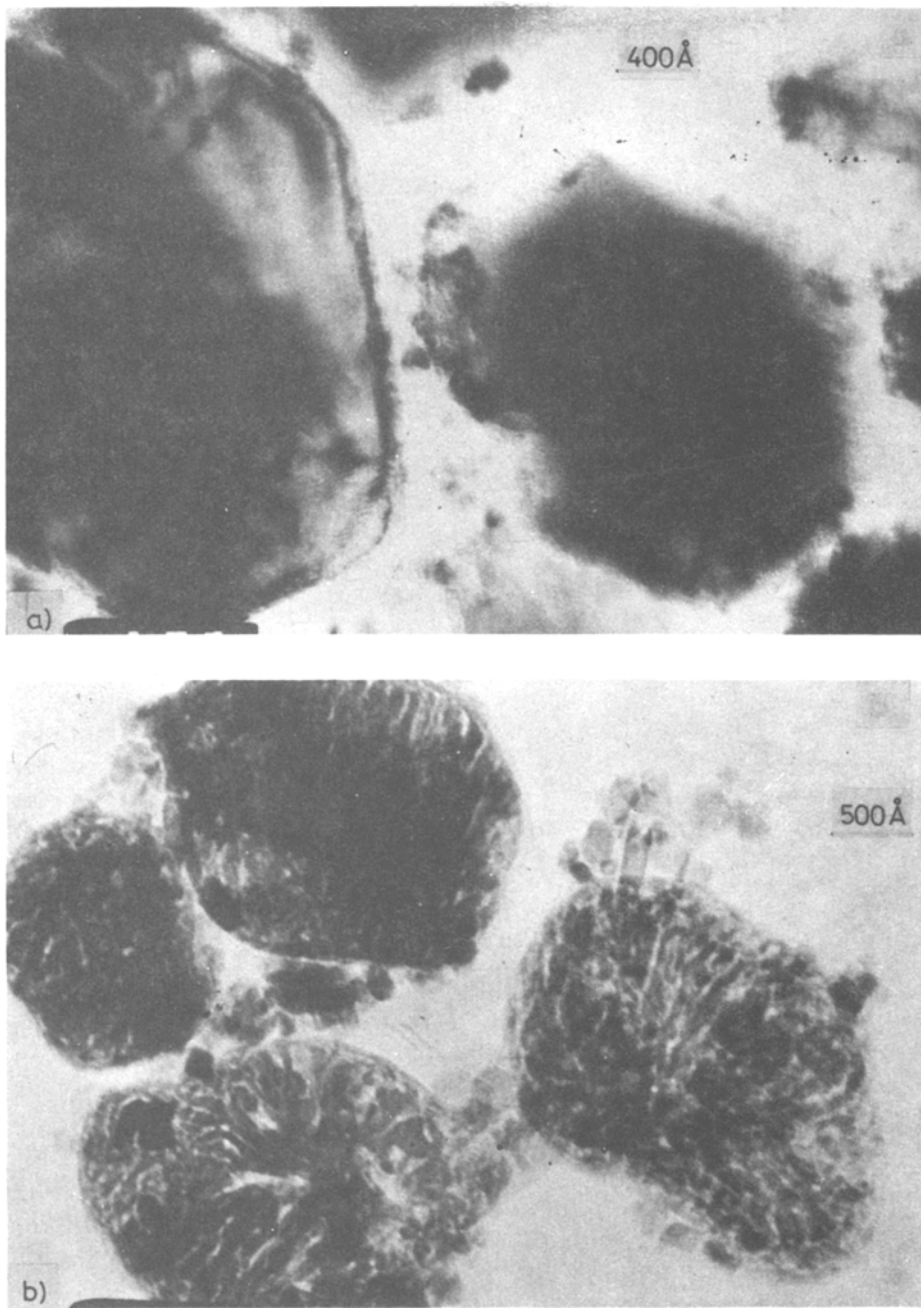
400Å
a)
500Å
b)

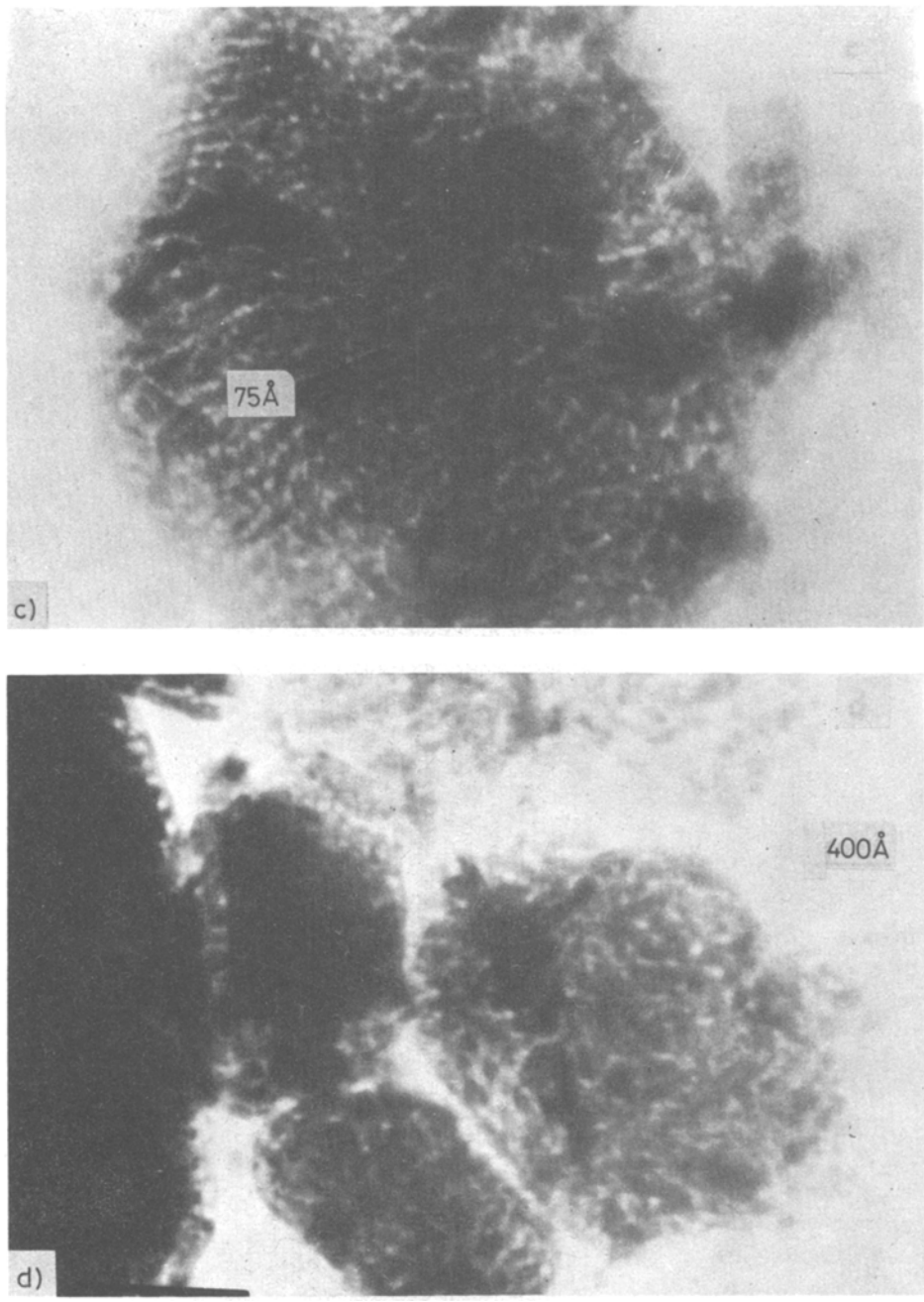

Fig. 4 Electron micrographs of a) undecomposed CoOOH, b) and c) partially decomposed sample (heated at 230°C, 1/2 hour), d) totally decomposed sample (heated at 300°, 1 hour)

Table 3 shows the results of the variance method applied to three selected profiles. It must be noted that peak to background ratios increase markedly with temperature and the values of maximum range of scan show a clear correlation with truncation errors ($\Delta k/k$), although this relationship depends also on crystallite shape [8]. For the sample heated at 300°, crystallite size (ϵ_k) varies from 53 to 93 Å, depending on the crystallographic directions, a behaviour indicative of a certain anisotropy in the growth of Co_3O_4 crystallites. These values are in good agreement with the domain size observed in Fig. 4b, c and d, that also reveals an heterogeneity in domain shapes.

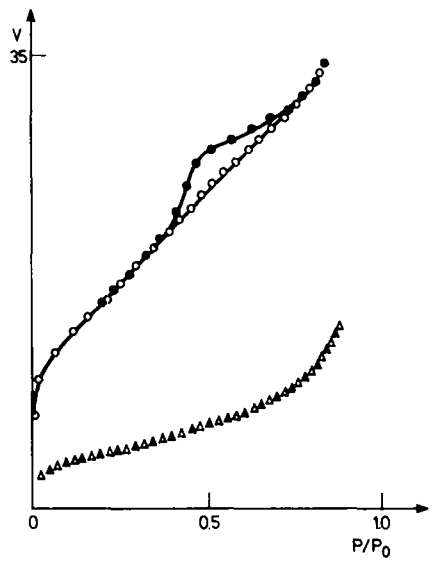

Fig. 5 N_2 adsorption isotherms of undecomposed CoOOH (△) and totally decomposed sample (heated at 300°, 1 hour) (○)

On the other hand, the analysis of microstrains shows an important anisotropy in this parameter. While the variance of the microstrain distribution is within the experimental error for the (220) line, a value of $5.23 \cdot 10^{-3}$ was calculated for the (511) reflection. These values show that crystallinity is not highly developed through some of the directions of the recently formed Co_3O_4 microcrystals. In this way, the absence of microstrains in the [220] direction could be interpreted by considering that the [110] direction of CoOOH remains unaltered when this phase is transformed into Co_3O_4, as Giovanoli et al. have pointed out [13].

On further heating, Co_3O_4 crystallites suffer a sintering process, in which anisotropy is lowered and crystallinity increases markedly, as it is manifested in Table 3.

On the above considerations, formal kinetics obtained from the analysis of both isothermal and non-isothermal weight loss data could be justified as follows. Of the three more significant mechanisms arising from the kinetic analysis – F_1, R_2, R_3 –, we can rule out the two interface mechanisms in which nucleation of the plates occurs preferentially at the corners and edges. The electron micrographs picture demonstrate

Table 3 Crystallite size and microstrains determination. Results of the variance method

Sample	h	k	l	σ_2/FWHM	P/Bk	$\Delta k/k$	$k \cdot 10^4$	$W_0 \cdot 10^6$		
	1	1	1	3.57	5.63	4.72	3.92	0.09		
850°C	2	2	0	3.58	9.95	3.69	3.87	0.22	g Profile	$\sqrt{\langle e^2 \rangle \cdot 10^3}$
	5	1	1	7.22	8.05	0.86	1.42	3.77	ϵ_k	
	1	1	1	3.77	3.31	7.21	6.58	−1.24	281	–
500°C	2	2	0	3.96	5.58	6.41	6.85	−1.74	279	–
	5	1	1	3.85	3.74	3.13	7.57	1.84	293	1.28
	1	1	1	3.44	1.54	11.71	30.36	−22.33	61	1.70
300°C	2	2	0	3.02	1.97	14.03	36.13	−34.61	53	–
	5	1	1	3.96	1.60	4.80	23.37	37.96	93	5.23

σ^2/FWHM: Maximum range of scan (in FWHM units).
P/Bk: Peak to background ratio.
$\Delta k/k$: Correction for truncation (percentage). } truncation corrected.
k: Slope of the variance-σ curves (rad). }
W_0: Intercept of the variance-σ curves (rad^2).
ϵ_k: Apparent crystallite size (Å). $\sqrt{\langle e^2 \rangle}$: Square root of the variance of the lattice strain distribution.

that the reaction takes place through a random nucleation process over the particle. The growth of these isolated nuclei originates the formation of cracks which divide the plates in coherently scattering domains of *ca.* 50–100 Å. These isolated blocks, initially of CoOOH, account for an unimolecular decay law, F_1, whether a single nucleus is generated on each crystallite [14] or a random nucleation develops in which each molecule possesses an equal probability for decomposition [15].

* * *

The authors wish to express their acknowledgement to ETSIA (Córdoba) and CSIC (Madrid) for their assessment in X-ray diffraction and electron microscopy studies, to CAICYT for financial support and Mrs. M. C. Mohedano for the drawing of the figures.

References

1 L. Hernan, J. Morales, A. Ortega and J. L. Tirado, J. Thermal Anal., 29 (1984) 479.
2 J. Zsakó, J. Phys. Chem., 72 (1968) 2406.
3 J. M. Criado, J. Morales and V. Rives, J. Thermal Anal., 14 (1978) 221.
4 S. Brunauer, P. H. Emmett and E. Teller, J. Am. Chem. Soc., 60 (1938) 1723.
5 H. J. Edwards and K. Toman, J. Appl. Cryst., 4 (1971) 332.
6 J. I. Langford, J. Appl. Cryst., 15 (1982) 315.
7 J. I. Langford and A. J. C. Wilson, in Crystallography and Crystal Perfection (G. N. Ramachandran, Ed.), 1963, p. 207.
8 A. W. Coats and J. P. Redfern, Nature, 208 (1964) 68.
9 P. K. Gallagher and D. W. Johnson, Jr., Thermochim. Acta, 6 (1973) 67.
10 L. K. Avramov, Thermochim. Acta, 15 (1976) 281.

11 T. Ozawa, Bull. Chem. Soc. Japan, 38 (1965) 1881.
12 H. E. Kissinger, Analyt. Chem., 29 (1957) 1702.
13 R. Ammann, W. Feitknecht and R. Giovanoli, VII. Congrès International de Microscopie Électronique, Grenoble, 1970, p. 467.
14 K. L. Mampel, Z. Phys. Chem., A187, 235 (1940).
15 P. W. M. Jacobs and F. C. Tompkins, in Chemistry of the Solid State (W. E. Garner, Ed.), p. 211, Academic Press, New York, 1955.

Zusammenfassung — Die Kinetik der thermischen Zersetzung von CoOOH im Vakuum wurde durch Analyse von dynamischen Gewichtsverlustdaten untersucht. Der Vergleich der Werte der durch verschiedene Methoden der Analyse von thermogravimetrischen und unter isothermen Bedingungen erhaltenen Daten läßt ein Gesetz erster Ordnung als den für die Reaktion am besten geeignetsten Mechanismus erkennen. Trotzdem ist keine klare Unterscheidung zwischen diesem Modell und auf geometrischen Gleichungen basierenden Modellen möglich. Die den Verlauf dieser Reaktion bestimmende formale Kinetik wurde auf der Basis der Röntgenprofilanalyse und elektronenmikroskopischer Ergebnisse ermittelt. Der Reaktion scheint ein statistischer Keimbildungsprozeß zugrunde zu liegen, der zur Bildung von kohärente Streubereiche von 50—100 nm begrenzenden Sprüngen führt. Dem Auftreten solcher isolierter Blöcke mag zuzuschreiben sein, daß die Zersetzungsgeschwindigkeit der Menge an unzersetztem Reaktant proportional ist.

Резюме — Кинетика реакции термического разложения CoOOH в вакууме была изучена на основе анализа данных динамической потери веса. Сопоставление значений энергий активации, вычисленных на основе различных методов анализа данных ТГ, с полученными в изотермических условиях, позволило обнаружить закон первого порядка, как наиболее приемлемый механизм реакции. Однако, нет ясного различия между этой моделью и моделями, основанными на геометрических уравнениях. Такая избирательность формальной кинетики была установлена на основании анализа профиля рентгеновских лучей и электронной микроскопии. Исследованная реакция сопровождается процессом произвольного образования центров кристаллизации, приводящих к образованию трещин, которые рождают когерентно-рассеивающие домены размера 5—10 нм. Появление этих изолированных блоков может объяснить скорость разложения пропорциональную количеству вещества, не подвергшегося разложению.